Strategy for Torque Ripple Reduction in IPMSM ⋆

Célio L. Filho * **Israel R. Soares** * **Khristian M. de Andrade Jr** *
Bernardo P. de Alvarenga * **Geyverson T. de Paula** *

* *Escola de Engenharia Elétrica, Mecânica e de Computação, Universidade Federal de Goiás (e-mail: eng.celiofilho@gmail.com, isr321@hotmail.com, khristianjr11@gmail.com, bernardo_alvarenga@ufg.br, geyverson@ufg.br).*

Abstract: The aim of this paper is to investigate the reluctance torque and to propose a novel control strategies to reduce the steady-state torque ripples in Interior Permanent Magnet Synchronous Machine (IPMSM). Despite the conventional vector control strategy applied to the PMSM use zero d_x-axis current to reduce the effect of the reluctance torque, this is unsuitable when it comes to the IPMSM due to the cross-coupling effect between the q_x- and d_x-axis. At first, a novel modeling of reluctance torque is proposes, which allows elaborating control strategy by means of injecting current in d_x-axis to null the reluctance torque together with the cogging torque. For this purpose, it is necessary the machine parameters and pre-made lookup table. The results demonstrate the effectiveness of the proposed strategy and that the torque ripple can be totally reduced.

Keywords: IPMSM, Finite Element Analysis (FEA), Reluctance Torque, Torque Ripple, Vector Control.

1. INTRODUCTION

One of the criteria to choose a machine is its torque capability and, mainly, how this torque can be delivered to the load/application with low torque ripple since torque ripple can produce vibration, mechanical stress (tear and wear), acoustic noise and represents loses. Within the Permanent Magnet Synchronous machines, the Interior one (IPMSM) stands out thanks to its torque production that is based on the permanent magnets and reluctance effects, this way, this machine has higher torque density and higher power density when compared to other types of radial-flux PMSM.

As for IPMSM, there are some intrinsic characteristics that affects the torque ripple: the cogging torque, the current waveform and its ripple as it is usually supplied by a voltage supply inverter (VSI); variation of the inductances (self-inductance and mutual inductance), which will produce the reluctance torque; and, finally, but not less important, the back-EMF waveform and its harmonic content.

In the IPMSM, the electromagnetic torque can be divided into: cogging torque, reluctance torque and mutual torque (Gieras, 2009; Hanselman, 2006). The cogging torque contributes to torque ripple only whereas the reluctance torque contributes to torque ripple and to the average torque value. Besides, the mutual torque that is due to the interaction between PM (back-EMF) and armature current, is the torque component with major electromagnetic torque average value contribution but it also produces torque ripple due to the interaction of the back-EMF harmonic content along with the armature current harmonic content.

The torque ripple can be predicted and mitigated by means of the machine design optimization process (Jahns and Soong, 1996; Chu and Zhu, 2013b; Bianchi and Bolognani, 2002; Jung et al., 2018) where the spatial harmonics are analyzed by means of Finite Element Analysis and optimized (Jung et al., 2018; Zhu and Howe, 2000; Bianchini et al., 2012; Güemes et al., 2011). However, the design optimization process may fail to create a torque ripple free machine or may not be enough since it can achieve a design solution that is not feasible due to the cost and manufacturing complexity.

On the other hand, the torque ripple reduction can be achieved by means of the machine control (Nakao and Akatsu, 2014; Lai et al., 2017; Matsui et al., 1991; Nakamura et al., 2009; de Castro et al., 2018; Houari et al., 2018; Ullah and Hur, 2020; Liu et al., 2018; Feng et al., 2019; Ren and Zhu, 2015; Luo and Liu, 2019; Bu et al., 2021; Liu et al., 2017; Kang et al., 2020). The machine control strategy commonly used for torque ripple minimization can be divided into two steps: first one, the torque ripple prediction; and the second one, the harmonic current compensation.

Usually, the reluctance torque modeling of a PMSM considers the ideal characteristics where the self-inductance and mutual inductance ripples are regardless, or the reluctance torque is described in two components: average value and ripple (Nakao and Akatsu, 2014; Chu and Zhu, 2013a).

⋆ This work was supported by CNPq, FAPEG and Coordenação de Aperfeiçoamento de Pessoal de Nível Superior - Brasil (CAPES) - Finance Code 001.

These considerations have led many researches around the world to express the reluctance torque with cross-coupled variables which is difficult to propose an analytical strategy for reluctance torque ripple reduction. This way, three different control strategies for electromagnetic torque ripple reduction are described and discussed in details here. For this purpose, a novel modeling of reluctance torque is approached, that involves fewer variables without using simplifications.

This paper is organized as follow: first, a review on extended dq axis (dq_x) is done, then, the electromagnetic torque modeling of IPMSM is presented. Next, a strategy for torque ripple reduction is proposed and an explanation of how the tests are carried out in IPMSM. In the last section, the results are presented and discussed.

2. EXTENDED DQ ($\mathrm{DQ_X}$) FOR VECTORIAL CONTROL

The vector control based on the classic dq transformation can be employed in machines with sinusoidal back-EMF, however, when it is used in a machine with non-sinusoidal back-EMF the results are not as good as the sinusoidal one due to the position estimation error since the position of the back-EMF vector does not coincide with the rotor angular position as in the sinusoidal one.

This way, in Oliveira et al. (2005) is proposed the vector control for machines with non-sinusoidal back-EMF using an extended version of the classic dq transformation. This extended version of dq is also known as dq_x. The application of dq_x transformation in variables on $\alpha\beta$ reference frame, $\mathrm{x}\alpha\beta$, results in variables in dq_x reference frame, x_dqx, as described by (1).

$$x_{dqx} = \frac{1}{a_x} e^{-j(\theta_x+\theta_m)}\, x_{\alpha\beta} \tag{1}$$

where a_x is the magnitude of dq_x transformation as expressed in (2); θ_x is the angle of dq_x transformation as expressed in (3); θ_m is the rotor angular position in electrical degree and $e_{\omega\alpha\beta}$ is the speed normalized back-EMF vector on $\alpha\beta$ reference frame.

$$a_x = \sqrt{\frac{3}{2}}\,\frac{1}{\sqrt{e_{\omega\alpha}^2 + e_{\omega\beta}^2}} \tag{2}$$

$$\theta_m + \theta_x = \arctan\left(\frac{-e_{\omega\alpha}}{e_{\omega\beta}}\right) \tag{3}$$

As can be noticed in (2) and (3), a_x and θ_x are not constant and are function of the rotor angular position and the back-EMF vector on stationary reference frame.

Through the definition of a reference torque, $T_{\mathrm{el}}^{\mathrm{ref}}$, the stator reference current vector in the dq_x reference frame can be calculated as in (4) and (5).

$$i_{qx}^{\mathrm{ref}} = \frac{T_{\mathrm{el}}^{\mathrm{ref}}}{a_x^2\, e_{qx}} \tag{4}$$

$$i_{dx}^{\mathrm{ref}} = k\, i_{qx} \tag{5}$$

where edq_x is the speed normalized back-EMF vector on dq_x reference frame and k is the ratio between i_{qx}^{ref} and i_{dx}^{ref} which is chosen to control the field enhancement or weakening.

This vector control strategy can be employed in sinusoidal and non-sinusoidal back-EMF, where in the sinusoidal machine $a_x = 1$ and $\theta_x = 0$ which shows that the dq reference frame is a particular case of dq_x reference frame.

3. ELECTROMAGNETIC TORQUE MODELING FOR IPMSM

The electromagnetic torque produced by IPMSM is resultant of the summation of three components: mutual torque, reluctance torque e cogging torque, as given by (6).

$$T_{\mathrm{el}} = T_{\mathrm{mutual}} + T_{\mathrm{reluctance}} + T_{\mathrm{cogging}} \tag{6}$$

The ripple presents in the components of the electromagnetic torque in (6) are undesirable and the mitigation of these ripples are the focus of the strategies presented in this work.

3.1 Mutual Torque

The mutual torque, T_{mutual}, is the interaction between the speed normalized back-EMF in ABC reference frame, e_A, e_B, e_C with the respective armature current in ABC reference frame i_A, i_B, i_C , as expressed by (7). When the back-EMF needs to be assessed in FEA with more accuracy it can be calculated as describe by de Paula et al. (2018).

$$T_{\mathrm{mutual}-ABC} = e_A\, i_A + e_B\, i_B + e_C\, i_C \tag{7}$$

In the case where the variables are in the dq_x reference frame, the mutual torque is expressed by (8).

$$T_{\mathrm{mutual}-dqx} = a_x^2\, (e_{qx}\, i_{qx} + e_{dx} i_{dx}) \tag{8}$$

Although the mutual torque is expressed as function of the speed normalized back-EMFs of q_x- and d_x- axis, i.e., e_{qx} and e_{dx}, the e_{dx} component will always be zero due to intrinsic characteristic of the dq_x transformation and, consequently, the mutual torque will depend only on a_x, e_{qx} and i_{qx}, simplifying (8).

3.2 Reluctance Torque

The reluctance torque, $T_{\mathrm{reluctance}}$, is due to the variation of self-inductance L_A, L_B, L_C and mutual inductance M_{AB}, M_{AC}, M_{BC} in ABC reference frame as function of the mechanical rotor position, θ_m, as expressed in (9).

$$\begin{aligned} T_{\mathrm{reluctance}-ABC} = \frac{1}{2}\left(i_A^2\,\frac{\partial L_A}{\partial \theta_m} + i_B^2\,\frac{\partial L_B}{\partial \theta_m} + i_C^2\,\frac{\partial L_C}{\partial \theta_m}\right) \\ + i_A\, i_B \frac{\partial M_{AB}}{\partial \theta_m} + i_B\, i_C \frac{\partial M_{BC}}{\partial \theta_m} + i_A\, i_C \frac{\partial M_{AC}}{\partial \theta_m} \end{aligned} \tag{9}$$

The variation of self-inductance L_A and mutual inductance M_{AB} (for instance) are calculated by means of (10) and (11) which employs a numerical method based on the concept shown in de Paula et al. (2018). This method, called on-load Inductance Derivative MST (Filho et al., 2020) is applied when it is desired a more accurate assessment of the variation of the inductances (self-inductance and mutual inductance) and it is used in the present paper to avoid numerical errors in FEA. In the same way as LA and MAB are calculated, the L_B, L_C, M_{AC}, M_{BC} are

also evaluated. Note that $M_{BA} = M_{AB}$, $M_{CA} = M_{AC}$ e $M_{CB} = M_{BC}$.

$$\left.\frac{\partial L_A}{\partial \theta_m}\right|_i = \frac{2\, l_{fe}\, r^2}{\mu_0} \int_0^{2\pi} (B_{i_A})_R \times (B_{i_A})_T \; d\theta \tag{10}$$

$$\begin{aligned}\left.\frac{\partial M_{AB}}{\partial \theta_m}\right|_i = &\frac{l_{fe}\, r^2}{\mu_0} \int_0^{2\pi} (B_{i_A})_R \times (B_{i_A})_T \; d\theta \\ &+ \frac{l_{fe}\, r^2}{\mu_0} \int_0^{2\pi} (B_{i_B})_R \times (B_{i_B})_T \; d\theta\end{aligned} \tag{11}$$

where l_{fe} is the active axial length of the electrical machine, r is the radius associated with the middle of the air gap, μ_0 is the permeability of free space, $(B_{PM})_R$ and $(B_{PM})_T$ are the radial and tangential components of PM flux density only in the middle of the air gap; $(B_{i_A})_R$ and $(B_{i_A})_T$ are the radial and tangential components of armature current flux density only due to phase A and θ is the angular position of flux density (radial and tangential) in the middle of the air gap.

Numerous authors consider the expression (12) to calculate the reluctance torque in dq_x reference frame, but in (12) the estimation of reluctance considers only the average value of the self-inductance and mutual inductance in the reference frame dq_x. Therefore, the ripple of the inductances is neglected. This formulation is derived from its counterpart in dq reference frame.

$$\begin{aligned}T_{\mathrm{reluctance}-dqx} = \frac{3}{2}\, p\, [&(L_{dx} - L_{qx})\; i_{dx}\, i_{qx} \\ &+ M_{dqx}\; (i_{qx}^2 - i_{dx}^2)]\end{aligned} \tag{12}$$

where p is the number of pole pairs, L_{qx}, L_{dx} are the self-inductance and M_{qx} is the mutual inductance in dq_x reference frame.

As the goal of this research is to consider the ripple present in reluctance torque, a improved formulation is proposed in (13). The main advantage of the usage of (13) is that the ripple and average value are together according to principle of conservation of energy in dq_x axis.

$$\begin{aligned}T_{\mathrm{reluctance}-dqx} = &\frac{1}{2} i_{dx}^2 \left.\frac{\partial L_{dx}}{\partial \theta_m}\right|_i + i_{dx}\, i_{qx} \left.\frac{\partial M_{dqx}}{\partial \theta_m}\right|_i \\ &+ \frac{1}{2} i_{qx}^2 \left.\frac{\partial L_{qx}}{\partial \theta_m}\right|_i\end{aligned} \tag{13}$$

The matrix of the variation of inductance in the reference frame ABC can be transformed to dq_x coordinates by means of (14).

$$\left[\left.\frac{\partial L_{dqx}}{\partial \theta_m}\right|_i\right] = [T_{dqx}] \left[\left.\frac{\partial L_{ABC}}{\partial \theta_m}\right|_i\right] \left[T_{dqx}^{-1}\right] \tag{14}$$

where,

$$T_{dqx} = \frac{1}{a_x}\sqrt{\frac{2}{3}} \begin{bmatrix} \sin(\theta'_x) & \sin\left(\theta'_x - \frac{2\pi}{3}\right) & \sin\left(\theta'_x + \frac{2\pi}{3}\right) \\ \cos(\theta'_x) & \cos\left(\theta'_x - \frac{2\pi}{3}\right) & \cos\left(\theta'_x + \frac{2\pi}{3}\right) \\ \sqrt{\frac{1}{2}} & \sqrt{\frac{1}{2}} & \sqrt{\frac{1}{2}} \end{bmatrix}$$

is the transformation matrix from ABC to dq_x and

$$T_{dqx}^{-1} = a_x \sqrt{\frac{2}{3}} \begin{bmatrix} \sin(\theta'_x) & \cos(\theta'_x) & \sqrt{\frac{1}{2}} \\ \sin\left(\theta'_x - \frac{2\pi}{3}\right) & \cos\left(\theta'_x - \frac{2\pi}{3}\right) & \sqrt{\frac{1}{2}} \\ \sin\left(\theta'_x + \frac{2\pi}{3}\right) & \cos\left(\theta'_x + \frac{2\pi}{3}\right) & \sqrt{\frac{1}{2}} \end{bmatrix}$$

is the inverse of transformation matrix from dq_x to ABC and $\theta'_x = \theta_m + \theta_x$.

3.3 Cogging Torque

The cogging torque, T_{cogging}, is the interaction of the magnetic flux of the rotor (due to the permanent magnets) with the edges of the stator teeth, wherein occurs variation of the reluctance according to the variation of the rotor position. The cogging torque can be estimated by means of FEM or measured according to IEEE (2015).

3.4 General Formulation of the Electromagnetic Torque

The general formulation of the electromagnetic torque commonly used is expressed in (15), wherein the magnetic flux can be separated in average value and its ripple. This formulation is derived from its counterpart in dq reference frame. It is important to observe the absence of the cogging torque whether it has been neglected or it is zero due to the design optimization of the machine.

$$T_{\mathrm{el}} = \frac{3}{2} p \left(i_{dx} \frac{d\Phi_{dx}}{d\theta_m} + i_{qx} \frac{d\Phi_{qx}}{d\theta_m} + \Phi_{dx} i_{qx} - \Phi_{qx} i_{dx} \right) \tag{15}$$

Where Φ_{qx} and Φ_{dx} are q_x- and d_x-axis flux linkages, respectively.

In (15), if the average values are considered and ripple is neglected, the expression (12) will be obtained. In some cases, wherein the stator current in d_x-axis is equal to zero, the mutual inductance is neglected and $L_{dx} \approx L_{qx}$, as in surface mounted PMSM, the electromagnetic torque is written as (16):

$$T_{\mathrm{el}} = \frac{3}{2}\, p\; (e_{qx}\, i_{qx}) \tag{16}$$

The general formulation of the electromagnetic torque can be described in the ABC reference frame by (17).

$$\begin{aligned}T_{\mathrm{el}} = &e_A\, i_A + e_B\, i_B + e_C\, i_C \\ &+ \frac{1}{2} \left(i_A^2 \frac{\partial L_A}{\partial \theta_m} + i_B^2 \frac{\partial L_B}{\partial \theta_m} + i_C^2 \frac{\partial L_C}{\partial \theta_m} \right) \\ &+ i_A\, i_B \frac{\partial M_{AB}}{\partial \theta_m} + i_B\, i_C \frac{\partial M_{BC}}{\partial \theta_m} + i_A\, i_C \frac{\partial M_{AC}}{\partial \theta_m} \\ &+ T_{\mathrm{cogging}}\end{aligned} \tag{17}$$

On the other hand, the general formulation of the electromagnetic torque proposed in this work is presented in (18). This formulation is based on (8), (13) and regards the cogging torque. As can be noticed, this formulation has a similar aspect of (17).

$$\begin{aligned}T_{\mathrm{el}} = &a_x^2\, e_{qx}\, i_{qx} \\ &+ \frac{1}{2} i_{dx}^2 \left.\frac{\partial L_{dx}}{\partial \theta_m}\right|_i + i_{dx}\, i_{qx} \left.\frac{\partial M_{dqx}}{\partial \theta_m}\right|_i \\ &+ \frac{1}{2} i_{qx}^2 \left.\frac{\partial L_{qx}}{\partial \theta_m}\right|_i + T_{\mathrm{cogging}}\end{aligned} \tag{18}$$

The advantage of (18) rather than (15) and (13) is the reduction of the number of variables in the formulation of the reluctance torque, making it easier to be handled and optimized according to the desired control strategy.

4. TORQUE CONTROL WITH STRATEGIES FOR REDUCTION OF THE ELECTROMAGNETIC TORQUE RIPPLE

The electromagnetic torque ripple has origin in the reluctance torque and the cogging torque, since the back-EMF is correctly orientated using dq_x reference frame. Thus, this work mitigates the electromagnetic torque ripple by means of injecting stator current in q_x- and d_x-axis in order to achieve the reference torque and to mitigate the torque ripple produced by the reluctance torque and cogging torque. It is important to highlight that the strategy proposed in this work are focused on the torque ripple in steady-state operation.

The harmonics present in the stator current in q_x- and d_x-axis are calculated by means of the proposed strategy elaborated based on the machine parameters. Next, the stator current is inserted into the dq_x vector control, Fig. 1. In the torque ripple minimization control the proposed strategy is separated in two steps: torque ripple prediction and harmonic current compensation.

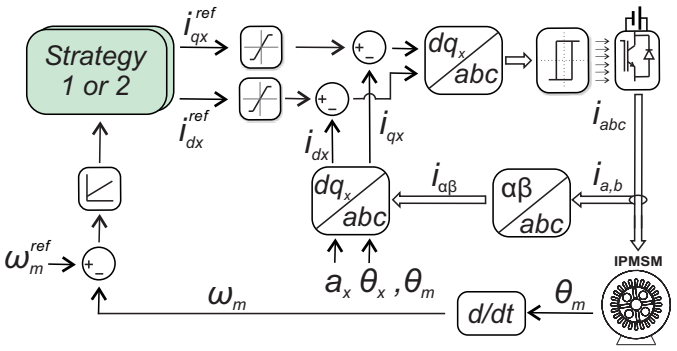

Figure 1. Schematic of insertion of the strategies in the dq_x control.

Firstly, the machine parameters are obtained through the formulations presented in the Section III for torque ripple prediction. The machine model is created in FEM software in order to simulate and to obtain the values and waveforms of the back-EMF, the inductance variation (self-inductance and mutual inductance) and cogging torque considering the saturation and cross-coupled effects that cannot be measured in the test bench. These variables will be used for reconstructing the values when requested by means of a look up table (LUT), afterwards, the variables will be used in each proposed strategy. Therefore, it is important to highlight that, for obtaining suitable data, the machine model built in FEM must have a good material characterization and a good mesh density. The FEM model has already been validated for the tested machine in other papers, showing a good agreement with the real one (Filho et al., 2020, 2018; Paiva et al., 2017).

During the analysis, the stator current, is, of each strategy will be evaluated by means of (19) in order to estimate whether the cooper loss of each strategy or to make a decision between two different d_x reference current values.

$$i_s = \sqrt{(i_{qx}^{\text{ref}})^2 + (i_{dx}^{\text{ref}})^2} \tag{19}$$

This way, it is possible to observe that an increase of i_{dx}, the stator current, is, increases, consequently. Thus, the higher the stator current, the higher copper loss.

4.1 Strategy 1: Conventional Control ($i_{dx} = 0$)

Usually, the dq_x control is employed with injecting only a q_x-axis armature current because this axis is responsible for producing the major part of the electromagnetic torque. Thus, d_x-axis current has null value due to the low contribution to the electromagnetic torque, mainly for surface mounted PMSM. The stator current in q_x- and d_x-axis are calculated by (4) and (5).

The aim of applying $i_{dx} = 0$ is based on analysis of the expression (19) which results in a lower stator current, is, and, consequently, lower copper loss. From the point of view of strategy for torque ripple reduction in IPMSM, the application of stator current with $i_{dx} = 0$ is interesting because it eliminates some parts of the reluctance torque, but the total elimination of the reluctance torque does not happen, according to (13) and (18).

If the $i_{dx} = 0$ in (13), the reluctance torque expression will be reduced, as given by (20). In addition, the expression (20) demonstrates that with $i_{dx} = 0$ still remains a part of the reluctance torque in the electromagnetic torque, which differs from the authors that consider (12) and (15). The expression (20) justifies why most of strategies based on (12) and (15) fail to mitigate the torque ripple or to improve the reluctance torque production in IPMSM.

$$T_{\text{reluctance}} = \frac{1}{2} i_{qx}^2 \left.\frac{\partial L_{qx}}{\partial \theta_m}\right|_i \tag{20}$$

4.2 Strategy 2: Reluctance Torque + Cogging torque = 0 in d_x-axis

The Strategy 2 uses the reluctance torque to cancel the cogging torque, i.e, the stator current in d_x-axis is responsible for cancelling the reluctance torque and the cogging torque.

The reference current in q_x-axis is calculated by means of (4) whereas the reference current in d_x-axis is calculated by (21).

$$\begin{aligned} &\frac{1}{2}\left(i_{dx}^{\text{ref}}\right)^2 \left.\frac{\partial L_{dx}}{\partial \theta_m}\right|_i + i_{dx}^{\text{ref}}\, i_{qx}^{\text{ref}} \left.\frac{\partial M_{dqx}}{\partial \theta_m}\right|_i \\ &\qquad + \frac{1}{2}\left(i_{qx}^{\text{ref}}\right)^2 \left.\frac{\partial L_{qx}}{\partial \theta_m}\right|_i + T_{\text{cogging}} = 0 \end{aligned} \tag{21}$$

The roots of (21) are found in (22)-(23) and they are the two possible d_x-axis reference current values for cancelling the reluctance torque and the cogging torque.

$$i_{dx}^{\text{ref}} = \frac{i_{qx}^{\text{ref}} \left(-\left.\frac{\partial M_{dqx}}{\partial \theta_m}\right|_i \pm \sqrt{\Delta} \right)}{\left.\frac{\partial L_{dx}}{\partial \theta_m}\right|_i} \tag{22}$$

$$\Delta = \left(\left.\frac{\partial M_{dqx}}{\partial \theta_m}\right|_i \right)^2 - \left.\frac{\partial L_{dx}}{\partial \theta_m}\right|_i \left.\frac{\partial L_{qx}}{\partial \theta_m}\right|_i - T_{\text{cogging}} \frac{\partial L_{dx}}{\partial \theta_m} \tag{23}$$

From (22)-(23), it can be seen that the d_x-axis reference current is not constant and varies according to the deriva-

tives of the self-inductance and mutual inductance and rotor position.

The values obtained in (22)-(23) for i_{dx} are applied in (19) and the one which i_s is lower is chosen.

The conditions (24) and (25) must be satisfied in order to (22) be a real number.

$$\left(\left.\frac{\partial M_{dqx}}{\partial \theta_m}\right|_i\right)^2 \neq \left.\frac{\partial L_{dx}}{\partial \theta_m}\right|_i \left.\frac{\partial L_{qx}}{\partial \theta_m}\right|_i \tag{24}$$

$$\left(\left.\frac{\partial M_{dqx}}{\partial \theta_m}\right|_i\right)^2 - \left.\frac{\partial L_{dx}}{\partial \theta_m}\right|_i \left.\frac{\partial L_{qx}}{\partial \theta_m}\right|_i > T_{\text{cogging}} \frac{\partial L_{dx}}{\partial \theta_m} \tag{25}$$

It is possible to determine the minimum value of i_{qx}^{ref} that satisfies the condition (25), which is expressed as (26):

$$i_{qx}^{\text{ref}} \geq \frac{T_{\text{cogging}} \dfrac{\partial L_{dx}}{\partial \theta_m}}{\left(\left.\dfrac{\partial M_{dqx}}{\partial \theta_m}\right|_i\right)^2 - \left.\dfrac{\partial L_{dx}}{\partial \theta_m}\right|_i \left.\dfrac{\partial L_{qx}}{\partial \theta_m}\right|_i} \tag{26}$$

5. RESULTS AND DISCUSSIONS

The torque control strategies are applied to the machine which test bench, rotor and cross-section are illustrated in Fig. 2. Yet, Table 1 shows the characteristics of this machine.

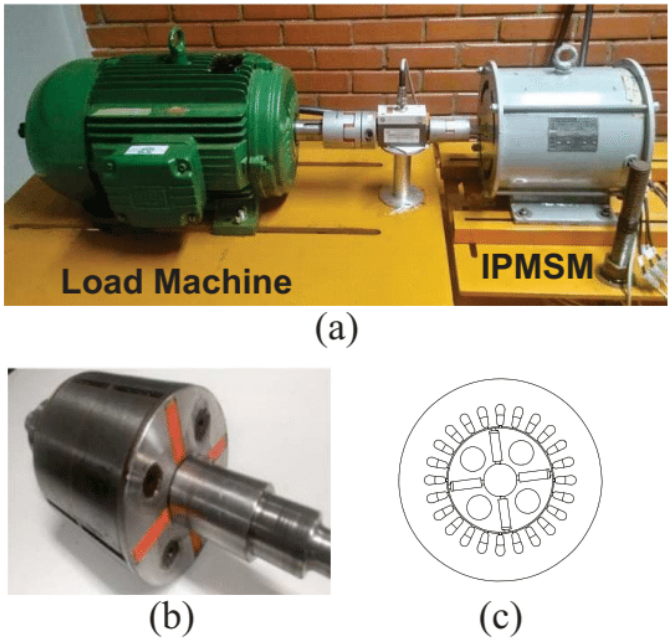

Figure 2. IPMSM (gray): (a) Test bench; (b) Rotor; (c) Cross-section.

The torque control is implemented according to the diagram proposed in Fig. 1, where is used a Proportional Integral (PI) controller in the speed loop with Proportional gain, $k_p = 20$, and Integral, $k_i = 200$. In this research is used the hysteresis controller for current loop due to its dynamic response and simplicity, with a hysteresis band of $\Delta i = 0.1$ A and the voltage source inverter have maximum switching frequency of 20 kHz. There are also current limiters in q_x- and d_x-axis of 8A. The reference speed is

Table 1. Characteristics of the machine

Parameter	Value	Parameter	Value
Slot number	24	Magnet thickness	0.8 mm
Pole number	4	Stator outer diameter	182 mm
Tooth width	8.16 mm	Stator inner diameter	96 mm
Slot opening	2.2 mm	Stator yoke width	22.9 mm
Shaft diameter	30 mm	Rotor outer diameter	94 mm
Tooth tip edge	1 mm	Voltage	220 V
Air-gap length	1 mm	Rated power	0.75 kW

to equal to 80 RPM and an 8 Nm load is applied to the motor.

As aforementioned, the values and waveforms of back-EMF, inductance derivatives (self-inductance and mutual inductance) and cogging torque for LUT are presented in Fig. 3, wherein are obtained according to the formulations of the Section III, based on FEA model and that have already been validated as discussed in Filho et al. (2020, 2018); Paiva et al. (2017).

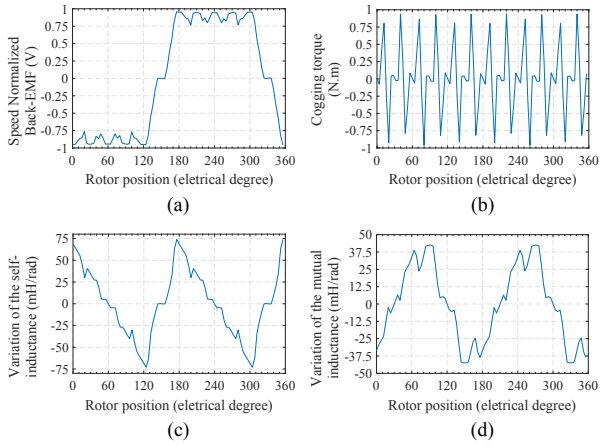

Figure 3. Parameters: (a) Back-EMF; (b) Cogging torque; (c) Variation of the self-inductance; (d) Variation of the mutual inductance.

In Fig. 4 are presented the results for Strategy 1 in steady-state. It is possible to notice that the torque ripple affects the speed. The stator current in q_x-axis have ripples similar as those presented in the torque and the stator current in d_x-axis is kept near the reference value (null).

Clearly, Strategy 1 cannot mitigate the torque ripple in IPMSM, which requires the proposal of other strategy as this paper proposes. Note that the electromagnetic torque of this strategy has maximum and minimum values of 9.32 and 6.54 Nm, respectively.

For comparison purposes, in all tests the machine is started with Strategy 1 and t = 1s the strategy is changed to the desired one. Thus, in all figures results is possible to compare and see the difference between Strategy 1 and the proposed strategy under investigation.

The Strategy 2 has two conditions described in (24) and (25) that must be satisfied. The condition (24) is satisfied, as can be seen in Fig. 5, and to satisfy the condition (25) for all rotor positions, the minimum current value of 1.6A for i_{qx}^{ref} must be reached, as given in (26) and as can be observed in Fig. 6.

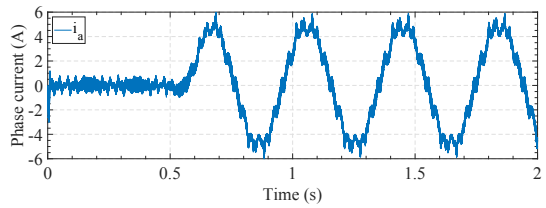

(a) Phase current (i_A)

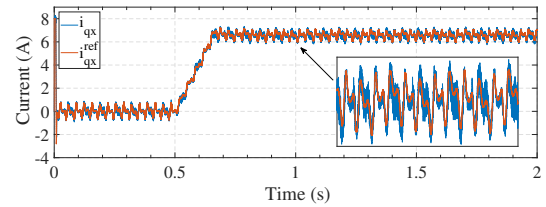

(b) i_{qx} current

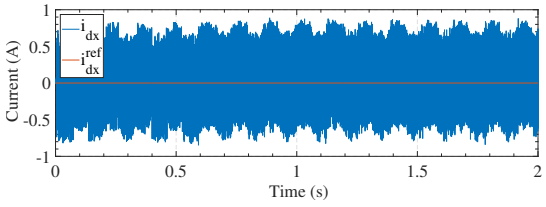

(c) i_{dx} current

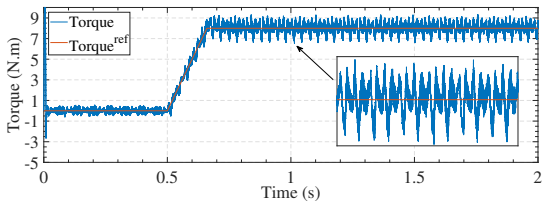

(d) Torque

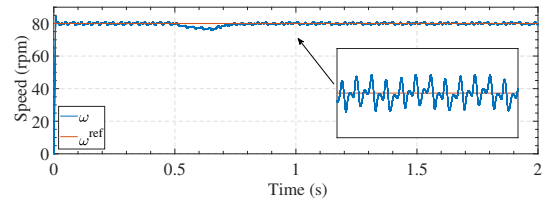

(e) Speed

Figure 4. Strategy 1: Conventional Control ($i_{dx} = 0$).

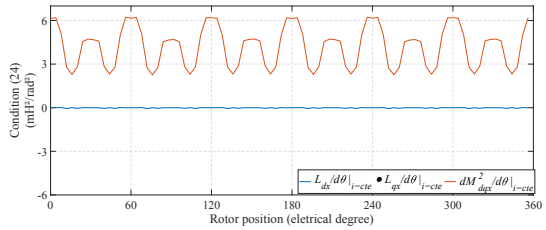

Figure 5. Check of the condition (24)

The conditions were satisfied since the minimum value of the assessed i_{qx}^{ref} for the desired reference torque ($T_{\text{el}}^{\text{ref}}$) is 6A. Therefore, it is possible to apply Strategy 2. Likewise, the Strategy 2 is implemented at t = 1s and the results obtained are presented in Fig. 7.

In Fig. 7, it is possible to observe that there is a change in the current waveform in d_x-axis as well in q_x-axis, when the Strategy 2 starts and the torque changes its behavior and has maximum and minimum 8.70 and 7.36 Nm, respectively.

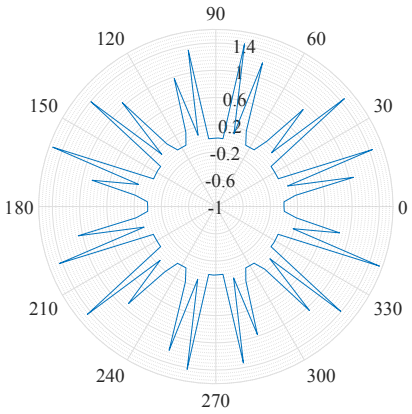

Figure 6. Minimum Value calculated for i_{qx}^{ref} based on (25)

Therefore, the torque ripple has been effectively reduced. The same effect can be seen for speed ripple.

For assessing the efficacy of the proposed strategies, the ripple factor, F_{ripple}, and the torque ripple, T_{ripple}, given by (27)-(28), are evaluated.

$$T_{\text{ripple}} = 100 \left(\frac{T_{\max} - T_{\min}}{T_{\text{average}}} \right) \tag{27}$$

$$F_{\text{ripple}} = \frac{T_{\text{CA (rms)}}}{T_{\text{average}}} \tag{28}$$

where $T_{\text{CA (rms)}}$ is the root mean square value of the ripple only, $T_{\min}$ is the minimum torque value, $T_{\max}$ is the maximum torque value and T_{average} is the average torque value.

The Table 2 presents the results obtained applying statistical parameter and calculations of (27) and (28) in the dynamic response of electromagnetic torque of the proposed strategy.

In Table 2 can be observed the torque ripple reduction in the proposed strategy when compared to Strategy 1. It is possible to see the increase of the minimum torque value, $T_{\min}$, and the reduction of maximum torque value, $T_{\max}$. In addition, the torque ripple and ripple factor indicate the ripple reduction in the electromagnetic torque by means of the reduction of their values. It is important to notice that the average torque value, T_{average}, of all strategies are equal to 8 N.m, the same as the load requires.

The Table 3 presents the results obtained applying statistical parameter in the stator current calculated by (19).

Table 2. Values regarding the electromagnetic torque.

Strategy	1	2
Average (N.m)	8.00	8.00
Maximum (N.m)	9.32	8.70
Minimum (N.m)	6.54	7.36
Ripple factor (%)	5.96	2.52
Torque ripple (%)	34.79	16.64

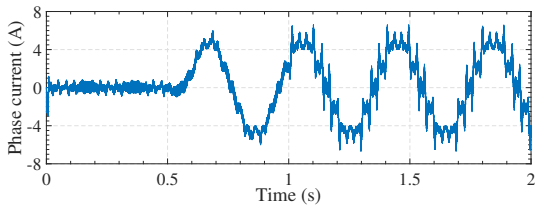

(a) Phase current (i_A)

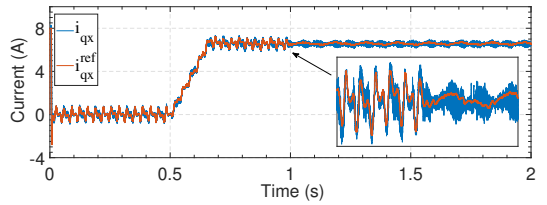

(b) i_{qx} current

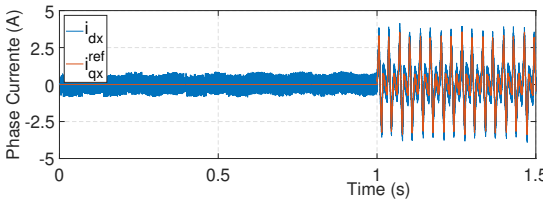

(c) i_{dx} current

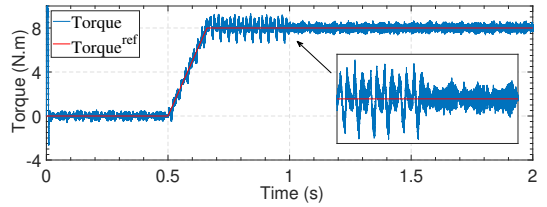

(d) Torque

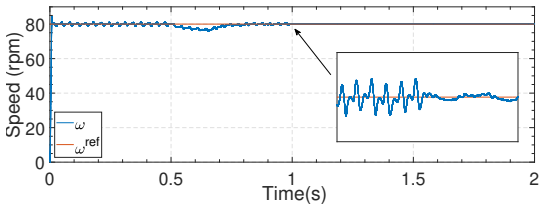

(e) Speed

Figure 7. Strategy 2: Reluctance Torque + Cogging Torque = 0 in d_x-axis

Table 3. Values regarding the i_s.

Strategy	1	2
Average (A)	6.55	6.70
RMS (A)	6.56	6.70
Maximum (A)	7.29	7.78
Minimum (A)	5.74	6.13

6. CONCLUSION

The new approach for reluctance torque modeling presented in this work reduces the number of variables in the description of the phenomenon (without simplifying the phenomenon), enabling the creation of torque ripple reduction strategies for IPMSM.

The Strategy 1 is interesting because of its simplicity. This strategy cancels two of three components of the reluctance torque and regarding the cogging torque, a design optimization process can be adopted for minimize this effect. But it will not be cost-effective and may fail.

In Strategy 2, the cogging torque and reluctance torque are canceled by means of the stator current in d_x-axis. As can be seen in the results presented in the work, this strategy is efficient but with operational limitations as for minimum stator current in d_x-axis.

REFERENCES

Bianchi, N. and Bolognani, S. (2002). Design techniques for reducing the cogging torque in surface-mounted pm motors. *IEEE Transactions on Industry Applications*, 38(5), 1259–1265. doi:10.1109/TIA.2002.802989.

Bianchini, C., Immovilli, F., Lorenzani, E., Bellini, A., and Davoli, M. (2012). Review of design solutions for internal permanent-magnet machines cogging torque reduction. *IEEE Transactions on Magnetics*, 48(10), 2685–2693. doi:10.1109/TMAG.2012.2199509.

Bu, F., Yang, Z., Gao, Y., Pan, Z., Pu, T., Degano, M., and Gerada, C. (2021). Speed ripple reduction of direct-drive pmsm servo system at low-speed operation using virtual cogging torque control method. *IEEE Transactions on Industrial Electronics*, 68(1), 160–174. doi:10.1109/TIE.2019.2962400.

Chu, W.Q. and Zhu, Z.Q. (2013a). Average torque separation in permanent magnet synchronous machines using frozen permeability. *IEEE Transactions on Magnetics*, 49(3), 1202–1210. doi:10.1109/TMAG.2012.2225068.

Chu, W.Q. and Zhu, Z.Q. (2013b). Reduction of on-load torque ripples in permanent magnet synchronous machines by improved skewing. *IEEE Transactions on Magnetics*, 49(7), 3822–3825. doi:10.1109/TMAG.2013.2247381.

de Castro, A.G., Pereira, W.C.A., de Almeida, T.E.P., de Oliveira, C.M.R., Roberto Boffino de Almeida Monteiro, J., and de Oliveira, A.A. (2018). Improved finite control-set model-based direct power control of bldc motor with reduced torque ripple. *IEEE Transactions on Industry Applications*, 54(5), 4476–4484. doi:10.1109/TIA.2018.2835394.

de Paula, G.T., de A. Monteiro, J.R.B., de Alvarenga, B.P., de Almeida, T.E.P., Pereira, W.C.A., and de Santana, M.P. (2018). On-load back emf of pmsm using maxwell stress tensor. *IEEE Transactions on Magnetics*, 54(7), 1–15. doi:10.1109/TMAG.2018.2829692.

Feng, G., Lai, C., Kelly, M., and Kar, N.C. (2019). Dual three-phase pmsm torque modeling and maximum torque per peak current control through optimized harmonic current injection. *IEEE Transactions on Industrial Electronics*, 66(5), 3356–3368. doi:10.1109/TIE.2018.2854550.

Filho, C., Assis, L., Alvarenga, B., and de Paula, G.T. (2018). Influence of vector control strategies on magnetic saturation and its effects on torque ripple of a pmsm. In *2018 13th IEEE International Conference on Industry Applications (INDUSCON)*, 1051–1058. doi:10.1109/INDUSCON.2018.8627225.

Filho, C., de Alvarenga, B.P., and de Paula, G.T. (2020). On-load apparent inductance derivative of ipmsm: Assessment method and torque estimation. *IEEE Transactions on Magnetics*, 56(4), 1–10. doi:10.1109/TMAG.2020.2973131.

Gieras, J. (2009). *Permanent Magnet Motor Technology: Design and Applications, Third Edition*. Electrical and Computer Engineering. CRC Press. URL `https://books.google.com.br/books?id=rFrFLUTri0MC`.

Güemes, J.A., Iraolagoitia, A.M., Del Hoyo, J.I., and Fernández, P. (2011). Torque analysis in permanent-magnet synchronous motors: A comparative study. *IEEE Transactions on Energy Conversion*, 26(1), 55–63. doi:10.1109/TEC.2010.2053374.

Hanselman, D. (2006). *Brushless Permanent Magnet Motor Design*. Magna Physics Publishing. URL `https://books.google.com.br/books?id=rilVPgAACAAJ`.

Houari, A., Bouabdallah, A., Djerioui, A., Machmoum, M., Auger, F., Darkawi, A., Olivier, J.C., and Benkhoris, M.F. (2018). An effective compensation technique for speed smoothness at low-speed operation of pmsm drives. *IEEE Transactions on Industry Applications*, 54(1), 647–655. doi:10.1109/TIA.2017.2740388.

IEEE (2015). Ieee trial-use guide for testing permanent magnet machines. *IEEE Std 1812-2014*, 1–56. doi:10.1109/IEEESTD.2015.7047988.

Jahns, T. and Soong, W. (1996). Pulsating torque minimization techniques for permanent magnet ac motor drives-a review. *IEEE Transactions on Industrial Electronics*, 43(2), 321–330. doi:10.1109/41.491356.

Jung, Y.H., Lim, M.S., Yoon, M.H., Jeong, J.S., and Hong, J.P. (2018). Torque ripple reduction of ipmsm applying asymmetric rotor shape under certain load condition. *IEEE Transactions on Energy Conversion*, 33(1), 333–340. doi:10.1109/TEC.2017.2752753.

Kang, S.W., Soh, J.H., and Kim, R.Y. (2020). Symmetrical three-vector-based model predictive control with deadbeat solution for ipmsm in rotating reference frame. *IEEE Transactions on Industrial Electronics*, 67(1), 159–168. doi:10.1109/TIE.2018.2890490.

Lai, C., Feng, G., Iyer, K.L.V., Mukherjee, K., and Kar, N.C. (2017). Genetic algorithm-based current optimization for torque ripple reduction of interior pmsms. *IEEE Transactions on Industry Applications*, 53(5), 4493–4503. doi:10.1109/TIA.2017.2704063.

Liu, G., Wang, J., Zhao, W., and Chen, Q. (2017). A novel mtpa control strategy for ipmsm drives by space vector signal injection. *IEEE Transactions on Industrial Electronics*, 64(12), 9243–9252. doi:10.1109/TIE.2017.2711507.

Liu, J., Gong, C., Han, Z., and Yu, H. (2018). Ipmsm model predictive control in flux-weakening operation using an improved algorithm. *IEEE Transactions on Industrial Electronics*, 65(12), 9378–9387. doi:10.1109/TIE.2018.2818640.

Luo, Y. and Liu, C. (2019). Multi-vector-based model predictive torque control for a six-phase pmsm motor with fixed switching frequency. *IEEE Transactions on Energy Conversion*, 34(3), 1369–1379. doi:10.1109/TEC.2019.2917616.

Matsui, N., Makino, T., and Satoh, H. (1991). Autocompensation of torque ripple of dd motor by torque observer. In *Conference Record of the 1991 IEEE Industry Applications Society Annual Meeting*, 305–311 vol.1. doi:10.1109/IAS.1991.178171.

Nakamura, K., Fujimoto, H., and Fujitsuna, M. (2009). Torque ripple suppression control for pm motor with high bandwidth torque meter. In *2009 IEEE Energy Conversion Congress and Exposition*, 2572–2577. doi:10.1109/ECCE.2009.5316344.

Nakao, N. and Akatsu, K. (2014). Suppressing pulsating torques: Torque ripple control for synchronous motors. *IEEE Industry Applications Magazine*, 20(6), 33–44. doi:10.1109/MIAS.2013.2288383.

Oliveira, A., de A. Monteiro, J., Aguiar, M., and Gonzaga, D. (2005). Extended dq transformation for vectorial control applications of non-sinusoidal permanent magnet ac machines. In *2005 IEEE 36th Power Electronics Specialists Conference*, 1807–1812. doi:10.1109/PESC.2005.1581876.

Paiva, R.D., Silva, V.C., Nabeta, S.I., and Chabu, I.E. (2017). Magnetic topology with axial flux concentration: A technique to improve permanent-magnet motor performance. *J. Microwaves, Optoelectron. Electromagn. Appl.*, 16(4), 881–899.

Ren, Y. and Zhu, Z.Q. (2015). Reduction of both harmonic current and torque ripple for dual three-phase permanent-magnet synchronous machine using modified switching-table-based direct torque control. *IEEE Transactions on Industrial Electronics*, 62(11), 6671–6683. doi:10.1109/TIE.2015.2448511.

Ullah, Z. and Hur, J. (2020). Analysis of inter-turn-short fault in an fscw ipm type brushless motor considering effect of control drive. *IEEE Transactions on Industry Applications*, 56(2), 1356–1367. doi:10.1109/TIA.2019.2961878.

Zhu, Z. and Howe, D. (2000). Influence of design parameters on cogging torque in permanent magnet machines. *IEEE Transactions on Energy Conversion*, 15(4), 407–412. doi:10.1109/60.900501.